

COLLIMATION OF ION BEAMS*

I. Strasik[#], O. Boine-Frankenheim, GSI Helmholtzzentrum für Schwerionenforschung, Darmstadt, Germany

Abstract

The SIS 100 synchrotron as part of the FAIR project at GSI will accelerate various beam species from proton to uranium. An important issue is to minimize uncontrolled beam losses using a collimation system. An application of the two-stage betatron collimation concept, well established for proton accelerators, is considered for the fully-stripped ion beams. The two-stage system consists of a primary collimator (a scattering foil) and secondary collimators (bulky absorbers). The main tasks of this study are: (1) to specify beam optics of the system, (2) to calculate dependence of the scattering angle in the foil on the projectile species, (3) to investigate importance of the inelastic nuclear interactions in the foil (4) to calculate momentum losses of the primary ions in the foil and (5) to estimate dependence of the collimation efficiency on the projectile species. A concept for the collimation of partially-stripped ions is based on the stripping of remaining electrons and deflecting using a beam optical element towards a dump location.

INTRODUCTION

Various beam dynamics processes can cause that particles enter into unstable orbits with large betatron amplitudes which leads to beam halo formation and emittance growth [1, 2]. The main reasons for halo formation are space charge, mismatched beam, nonlinear forces, RF noise, magnet errors, scattering, resonances, beam-beam effects and electron clouds [1, 2]. Beam halo is one of the reasons for uncontrolled beam-loss interacting with accelerator structures. Uncontrolled beam loss causes the following problems: vacuum degradation due to desorption process, superconducting magnets quenches, activation of the accelerator structure, radiation damage of the equipment and devices [1]. The main purpose of the collimation system is to remove the halo, consequently to reduce above mentioned problems and to provide a well defined and shielded storing location for the beam losses.

The halo collimation system in future SIS 100 synchrotron of FAIR (Facility for Antiproton and Ion Research) must be capable to collimate various ion species from proton up to uranium [3]. The situation is even more complicated due to operation with partially- (e.g. $^{238}\text{U}^{28+}$) and fully- (e.g. $^{40}\text{Ar}^{18+}$) stripped ions. In case of the proton and light-ion beams the collimation system is required in order to limit the residual activation of accelerator components. A tolerable level of uncontrolled beam-losses is 1 W/m for protons [4]. The tolerable losses for other ion species are estimated in Ref [5]. In case of the heavy ions the main issue is the vacuum degradation due to desorption [6] as well as the radiation damage [7].

*Work supported by BMBF and EU program EuCARD, WP8, ColMat
[#]i.strasik@gsi.de

For proton and light fully-stripped ion beams a well established two-stage betatron collimation system [8-11] was adopted for transverse collimation in SIS 100. The collimation concept for the partially-stripped heavy ions is rather different. It is based on the change of the charge state of the halo particles using a stripping foil. Consequently the stripped ions can be deflected toward a dump location using a beam optical element.

TWO-STAGE BETATRON COLLIMATION

The two-stage collimation system consists of: a) a primary collimator (a thin foil) which scatters the halo particles and b) secondary collimators (bulky blocks) which are necessary to absorb the scattered particles (secondary halo) [8-11]. It is not desirable to intercept the halo particles directly by the secondary collimators. For this reason they are located further from the beam envelope than the primary collimator by a so-called "retraction distance", $\delta = n_s/n_p - 1$, where n_p and n_s are the normalised apertures of the primary and secondary collimators, respectively. Optimal phase advances for maximum collimation efficiency at certain values of n_p and n_s can be calculated using the formulas:

$$\mu_{S1} = \arccos \frac{n_p}{n_s} \quad \mu_{S2} = \pi - \mu_{S1}, \quad (1)$$

where μ_{S1} and μ_{S2} is the phase advance between the primary – 1st secondary and primary – 2nd secondary collimator, respectively.

Detailed beam-optics specifications of the two-stage collimation system in 1D and 2D are derived by Trenkler and Jeanneret [8, 9] and Seidel [10].

1D Optics

In order to specify the two-stage collimation system we use normalized particle coordinates X and X' :

$$\begin{pmatrix} X \\ X' \end{pmatrix} = \frac{1}{\sigma_x} \begin{pmatrix} 1 & 0 \\ \beta_x & \alpha_x \end{pmatrix} \begin{pmatrix} x \\ x' \end{pmatrix} \quad \sigma_x = \sqrt{\beta_x \varepsilon_x}, \quad (2)$$

where x and x' are the coordinates in the horizontal plane, α_x and β_x are the Twiss parameters and ε_x is the beam emittance in the x transverse plane. Transport of the particles in the normalized phase space from the primary collimator to the secondary collimators can be calculated using the 2×2 transfer matrix M :

$$\begin{pmatrix} X_S \\ X'_S \end{pmatrix} = M \begin{pmatrix} X_P \\ X'_P \end{pmatrix} \quad M = \begin{pmatrix} \cos \mu_S & \sin \mu_S \\ -\sin \mu_S & \cos \mu_S \end{pmatrix}, \quad (3)$$

where μ_S is the phase advance between the primary and the 1st or 2nd secondary collimator [8, 9].

The amplitude of a particle in the corresponding plane is defined as $a = \sqrt{X^2 + X'^2}$. The normalised particle coordinates at the primary collimator before scattering are considered to be $X_P = n_P$ and $X'_P = 0$, or the real coordinates are $x = n_P \sigma_x$ and $x' = -(\alpha/\beta)x$.

The minimal angle $X' = k$ which a particle must have after scattering in the primary collimator in order to be intercepted by the secondary collimators is defined as follows:

$$k = \frac{n_S - n_P \cos \mu_S}{\sin \mu_S}. \quad (4)$$

The angle k_{opt} calculated for the optimal phase advances (see Eq. 1), is then expressed as [8, 9]:

$$k_{opt} = \sqrt{n_S^2 - n_P^2} = n_P \sqrt{2\delta + \delta^2}. \quad (5)$$

Figure 1 shows phase space plots at the primary collimator (P) and at the secondary collimators (S1 and S2). It can be seen how the particles scattered outwards from and towards to the beam centre are collimated by the secondary collimators. Both secondary collimators are located at the optimal phase advances for the interception of the maximum number of scattered particles. In Figure 1 the angle k_{opt} is presented as the red and green point for the first and second secondary collimator, respectively. The minimal amplitude of a particle which is intercepted by the secondary collimators is then:

$$a_{min} = \sqrt{n_P^2 + k_{opt}^2} = n_S. \quad (6)$$

The scattered protons populate a selected region of the phase space, namely a straight line. This means that the scattering process adds a random kick only to X' and Y' (angles) but not to X and Y (positions) [8-10].

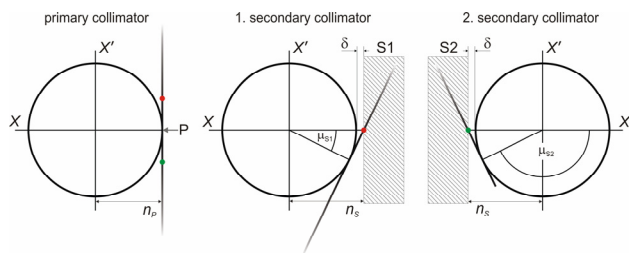


Figure 1: Normalized phase space plots at the collimators.

2D Optics

Since the scattering of the halo particles in the primary collimator is an isotropic process and occurs in both planes, horizontal and vertical, the 2D description of the two-stage collimation system is required [8-11]. It was found out that an optimal geometry for the efficiency of

the system is a circular or elliptical aperture of the collimators [8, 9]. A rectangular shape was found to be less efficient [8]. Since accelerators have to operate at various beam energies the aperture of the collimation system should be adjustable. This is not mechanically possible with a circular aperture. However, a sufficient result can be reached with an octagonal approximation of the circular shape [8, 9].

The impact point of the halo particles is again assumed to be at the edge of the circular primary collimator and betatron oscillations in both planes are at their maxima. The normalized particle coordinates are then specified as:

$n_P = \sqrt{X^2 + Y^2}$ and $X' = Y' = 0$. The normalized coordinates are grouped into a vector $\vec{V} = (X, X', Y, Y')$

which is transported between two locations with the 4×4 transfer matrix M . The transfer matrix consists of two clockwise rotations, one for the horizontal and one for the vertical plane where the angles of rotations μ_X and μ_Y , are the betatron phase advances [9]. For the calculation of the k_{opt} which is again the smallest scattering angle intercepted by the secondary collimators we get again the Equation 5. The k_{opt} can be factorized as follows:

$$k_{opt} = k_{X,opt} \cos \phi + k_{Y,opt} \sin \phi, \quad (7)$$

which is the normalized equation of a line with k_{opt} being the shortest distance to the origin and ϕ is its slope. ϕ is the scattering angle in polar coordinates [9].

COLLIMATION OF FULLY-STRIPPED IONS

For the transverse halo collimation of fully-stripped ions in SIS 100 an application of the two-stage betatron collimation system is considered. The primary collimator is assumed to be 1 mm thick tungsten foil. The main goal is to find out if the collimation system originally designed for protons can be used also for the fully-stripped ions. In order to do this, the following processes and their dependence on the ion species must be investigated:

- scattering of the halo particles in the primary collimator,
- inelastic nuclear interactions of the particles with the nuclei of the primary collimator,
- energy losses of the particles in the primary collimator.

These processes have direct impact on the collimation efficiency and it is reasonable to perform the calculations for some reference physical quantity related to the beam parameters. The magnetic rigidity, $B\rho = p/q$ where p is the momentum and q is the charge of the particle, was chosen as the reference quantity because it relates to the injection and extraction energy of the beam. The magnetic rigidity dependence on the kinetic energy of the beam for various ion species from proton up to $^{40}\text{Ar}^{18+}$ is presented in Figure 2. The dashed lines represent the maximum rigidities for the synchrotrons SIS 18 and SIS 100. The synchrotron SIS 18 will be a booster for SIS 100 [3].

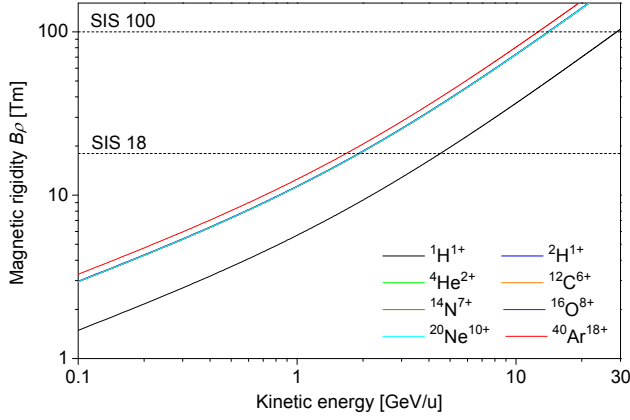


Figure 2: Dependence of the magnetic rigidity on the kinetic energy of the beam.

Scattering of the Halo Particles in the Primary Collimator

Scattering of high energy particles interacting with the nuclei in a thin foil can be well described by Molière's theory of multiple Coulomb scattering [12]. The angular distribution of the scattered particles downstream of the foil is roughly Gaussian for small deflection angles. The rms angle of the projected distribution is given by:

$$\theta_{rms} = \frac{13.6}{\beta c p} Z \sqrt{\frac{L}{L_R}} \left[1 + 0.038 \cdot \ln\left(\frac{L}{L_R}\right) \right], \quad (8)$$

where p , β , c and Z are the momentum, beta relativistic parameter, speed of light and proton number of the incident particle, respectively. The parameter L is the thickness of the target and L_R is the radiation length of the particle in the target material [12].

The θ_{rms} deflection angle was calculated for $^1\text{H}^{1+}$, $^2\text{H}^{1+}$, $^4\text{He}^{2+}$, $^{12}\text{C}^{6+}$, $^{14}\text{N}^{7+}$, $^{16}\text{O}^{8+}$, $^{20}\text{Ne}^{10+}$ and $^{40}\text{Ar}^{18+}$ primary ions scattered by 1 mm thick tungsten foil. The dependence of θ_{rms} on the magnetic rigidity is presented in Figure 3.

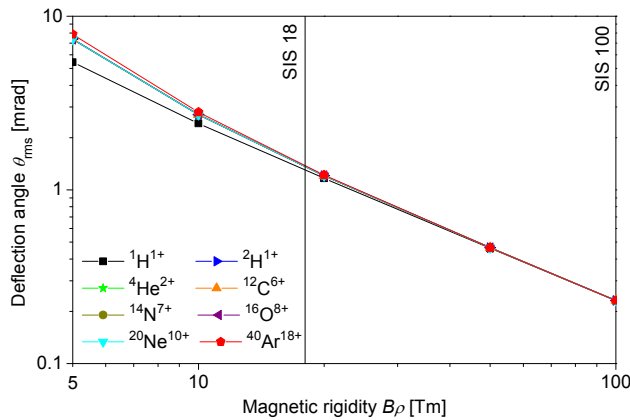


Figure 3: Dependence of the projected deflection angle θ_{rms} on the magnetic rigidity for the particles scattered in the 1 mm thick tungsten foil.

One can observe that at lower rigidities θ_{rms} for the heavier ions is larger than for protons. Towards the higher rigidities θ_{rms} for protons and heavier ions starts to coincide and above 20 Tm the values are practically the same. Already at the SIS 18 maximum rigidity (18 Tm), the θ_{rms} values are very similar for all considered ion species. This is due to the fact that momentum p for various ion species at the same magnetic rigidity is increasing with the charge number q of the particle (for fully-stripped ions $q = Z$). However, p is also in the denominator of Equation 8 which itself depends on the Z of the particle. θ_{rms} is larger for heavier projectiles at lower rigidities due to the smaller β relativistic parameter.

Probability of Inelastic Nuclear Interaction in the Primary Collimator

Cross sections for the inelastic nuclear interaction σ_{in} at $E_K > 100$ MeV/u was calculated using Sihver formula:

$$\sigma_{in} = \pi r_0^2 \left[A_p^{1/3} + A_t^{1/3} - b_0 (A_p^{-1/3} + A_t^{-1/3}) \right]^2, \quad (9)$$

$$b_0 = g - h (A_p^{-1/3} + A_t^{-1/3})$$

where $r_0 = 1.36 \times 10^{-15}$ m, A_p and A_t are the projectile and the target-nuclei mass numbers. The parameter g is equal to 2.247 and 1.581 for proton-nucleus and nucleus-nucleus interaction, respectively. The parameter h is equal to 0.915 and 0.876 for proton-nucleus and nucleus-nucleus interaction, respectively [13].

Using the cross section σ_{in} the mean free path λ for the inelastic nuclear interaction can be calculated as $\lambda = A_t / (\rho_t N_A \sigma_{in})$ where A_t is the target-nuclei mass number, ρ_t is the density of the target material and N_A is the Avogadro constant. The probability of the inelastic nuclear interaction is then expressed as $P = 1 - \exp(-L/\lambda)$ where L is the thickness of the target. The probability P was calculated in tungsten foils with various thicknesses for ion species again from $^1\text{H}^{1+}$ up to $^{40}\text{Ar}^{18+}$ (see Fig. 4). It can be seen that the probability P for 1 mm thick foil varies between 0.010 ($^1\text{H}^{1+}$) and 0.026 ($^{40}\text{Ar}^{18+}$).

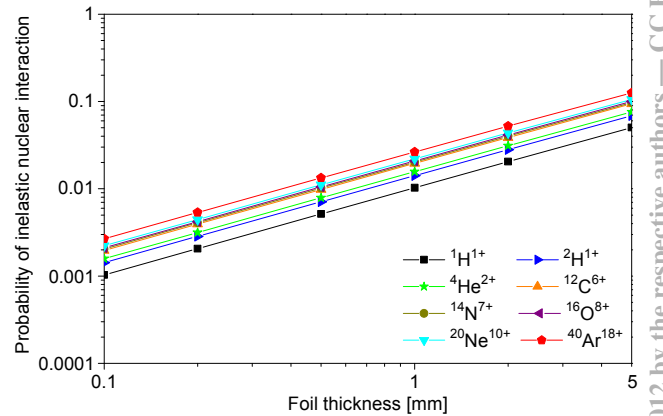


Figure 4: Probability of inelastic nuclear interaction in a tungsten foil with various thickness for $E_K > 100$ MeV/u.

Momentum Losses in the Primary Collimator

Energy losses and consequently the momentum losses can be calculated using the Bethe formula:

$$-\frac{dE}{dx} = \frac{nZq^2 4\pi\alpha^2 \hbar^2}{m_e \beta^2} \left[\ln \left(\frac{2m_e c^2 \beta^2}{I(1-\beta^2)} \right) - \beta^2 \right], \quad (10)$$

where n is number of atoms with proton number Z per cubic metre, q is the charge of the particle, α is the fine structure constant, $\hbar = h/2\pi$ where h is the Planck constant, m_e is the rest mass of the electron, β is the relativistic parameter, c is the speed of light and I is the mean ionization potential.

In Figure 5 the momentum losses in 1 mm thick tungsten foil for various projectiles are presented. The losses vary from about 4.4×10^{-4} for protons up to 8.1×10^{-3} for $^{40}\text{Ar}^{18+}$ ions at the maximum rigidity of SIS 18.

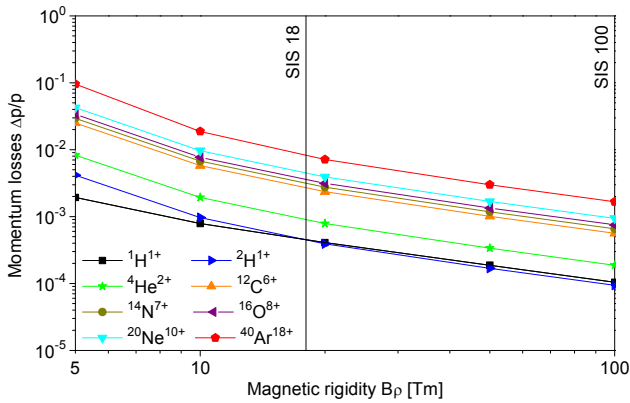


Figure 5: Momentum losses in 1 mm thick primary collimator made of tungsten.

The influence of the momentum losses in the primary collimator on the efficiency of the collimation system has been studied analytically in Refs. [8, 9]. We have to first specify the normalized dispersion χ and χ' :

$$\begin{pmatrix} \chi \\ \chi' \end{pmatrix} = \frac{1}{\sigma_x} \begin{pmatrix} 1 & 0 \\ \beta_x & \alpha_x \end{pmatrix} \begin{pmatrix} D \\ D' \end{pmatrix}, \quad (11)$$

where D and D' is the real dispersion. For simplicity we assume that the particle scattered in the primary collimator has original momentum deviation $dp/p = 0$ and its coordinates before scattering are again $X_p = n_p$ and $X'_p = 0$. Due to the interaction with the primary collimator the particle is deflected by the angle k and loses a fraction of its original momentum which is equal to $dp/p = \delta$. The coordinates of the particle behind the primary collimator then change to $X_p = n_p - \delta\chi_p$ and $X'_p = k - \delta\chi'_p$. Transport of the particle towards the secondary collimators is then calculated as $X_s = X_p \cos \mu_s + X'_p \sin \mu_s + \delta\chi_s$ [8, 9]. For the k we get:

$$k = \frac{n_s - n_p \cos \mu_s}{\sin \mu_s} + \delta \frac{\chi_p \cos \mu_s - \chi_s}{\sin \mu_s} + \delta \chi'_p. \quad (12)$$

If the collimation system is located in a straight section without dipole magnets the dispersion function follows the beta function and the dispersion vector simply rotates in the normalized phase space by the phase advance $\chi_s = \chi_p \cos \mu_s + \chi'_p \sin \mu_s$. Inserting this formula to Eq. 12 we get:

$$k = \frac{n_s - n_p \cos \mu_s}{\sin \mu_s}, \quad (13)$$

and for the optimal phase advances between the collimators we get again $k_{opt} = \sqrt{n_s^2 - n_p^2} = n_p \sqrt{2\delta + \delta^2}$ [8, 9]. There are some important consequences of this result. The first is that the optimal angle k_{opt} does not depend on the momentum losses if the whole collimation system is placed in a straight section free of dipoles. Another consequence is that particles with significant momentum losses which are not intercepted by the secondary collimators will be very likely lost in the following arc section with dipole magnets [8, 9].

COLLIMATION OF PARTIALLY-STRIPPED IONS

In order to reach high intensities of heavy ion beams SIS 100 will be operated with partially-stripped ions of intermediate charge states. For instance the heavy ions of the following charge states are considered: $^{238}\text{U}^{28+}$, $^{197}\text{Au}^{25+}$, $^{181}\text{Ta}^{24+}$, $^{132}\text{Xe}^{22+}$ or $^{84}\text{Kr}^{17+}$. With the intermediate charge states operation beam intensities above 10^{11} ions per cycle can be reached [3, 14]. However, halo formation and consequently uncontrolled losses of the high-intensity heavy ion beams can cause specific problems such as vacuum degradation due to ion induced desorption [6, 14] and radiation damage [7].

The concept considered for the halo collimation of the partially-stripped ions is based on the charge state exchange of the primary ions using a stripping foil. The stripped ions are consequently deflected towards a dump location using a beam optical element. The stripping foil is planned to be located in the slow extraction area of the SIS 100. The reason is that a part of the partially-stripped heavy ions interact directly with the electrostatic septum wires (passing through) during the slow extraction. These ions are then assumed to change their charge state to be close to the fully-ionized due to the stripping process in the wires. It was found out in previous studies that most of the fully-stripped particles are then lost at the two quadrupoles and the collimator between them behind the slow extraction septum [7]. For this reason it was decided that the two quadrupoles originally designed as superconducting as all the rest in the SIS 100 lattice, will be changed for the warm version in order to avoid the quenches [7]. This fact can be

utilized also in the halo collimation design of the partially-stripped heavy ions. The primary collimator (a stripping foil) is placed in front of the quadrupole doublet in the slow extraction area. The intermediate charge-state heavy ions are stripped of their remaining electrons and are then intercepted by the warm quadrupoles and the collimator between them which play the role of the absorbers.

A detailed theoretical and experimental study of the charge exchange of the partially-stripped heavy ions is presented in Ref. [15]. Using this approach implemented in the code GLOBAL the equilibrium charge state distribution of four partially-stripped heavy ions namely ^{238}U , ^{197}Au , ^{181}Ta , ^{132}Xe and ^{84}Kr , was calculated (see Fig. 6). The calculations were performed for 500 μm thick titanium foil at beam injection energy and at high beam energies. It can be seen that in both cases the equilibrium state is close to the fully ionized state.

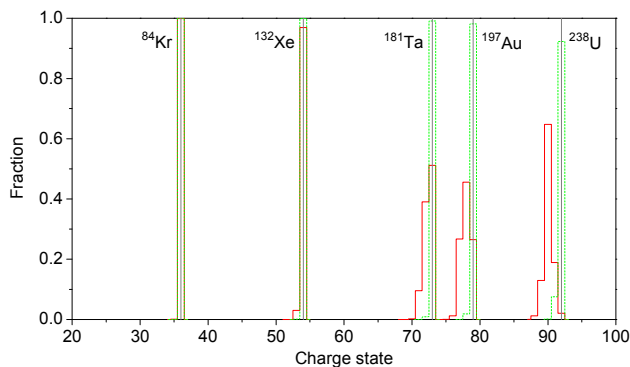


Figure 6: Charge state distribution for Kr, Xe, Au and U ions interacting with 500 μm thick titanium foil at the injection beam energy (red solid lines) and at the high beam energies (green dashed lines). The fully ionized state is represented by the grey vertical solid line.

CONCLUSIONS

Halo collimation of partially- and fully- stripped ions was studied. Dependence of the collimation efficiency on the scattering, inelastic nuclear interaction and momentum losses in the primary collimator was calculated. These processes were investigated for the various ion species at the same magnetic rigidity.

It was found out that at low rigidities the scattering angle for the heavier ions is larger than for protons. Towards the higher rigidities the scattering angle for protons and heavier ions starts to coincide and above 20 Tm the values are all very similar. This means that at high rigidities the scattering of various ion species from protons up to argon ions in the primary collimator has almost no influence to the collimation efficiency.

The inelastic nuclear interactions in the considered primary collimator have also very low influence to the collimation efficiency. It was found out that the probability of inelastic nuclear interaction even for ^{40}Ar ions is less than 3 % in the 1 mm thick primary collimator

made of tungsten. The probability is decreasing with the decreasing the mass number of the particles.

Influence of the momentum losses in the primary collimator is also not significant if the collimation system is localized in a straight section with no dipole magnets. However the particles with large momentum losses which are not intercepted by the secondary collimators will be likely lost in the following arc section of the accelerator.

The collimation efficiency was considered as the ratio of the particles intercepted by the secondary collimators to the number of particles scattered on the primary collimator. However the particles which escape can be intercepted in the next turns. For a more realistic estimation of the collimation efficiency, i.e the ratio of the particles intercepted by the collimation system to the total number of the lost particles, a detailed particle tracking and calculation of the beam loss distribution in the synchrotron using simulation codes is needed.

The collimation concept for the partially-stripped ions is based on the stripping of their remaining electrons and consequently their interception by the two warm quadrupoles in the slow extraction area of SIS 100.

REFERENCES

- [1] K. Wittenburg, "Beam halo and bunch purity monitoring", CERN Accelerator School: Course on Beam Diagnostics, Dourdan, France, June 2008, p. 557 (2008).
- [2] A.V. Fedotov, Nucl. Instrum. Methods Phys. Res. Sect. A 557 (2006) 216.
- [3] H.H. Gutbrod (Editor in Chief), FAIR - Baseline Technical Report, GSI Darmstadt, (2006).
- [4] N.V. Mokhov and W. Chou (Eds), Proc. of the 7th ICFA Mini-Workshop on High Intensity High Brightness Hadron Beams, Wisconsin, USA, 1999, p. 3. (edited by FNAL, Batavia, Illinois, 2000).
- [5] I. Strasik, E. Mustafin and M. Pavlovic, Phys. Rev. ST Accel. Beams 13 (2010) 071004.
- [6] E. Mahner, Phys. Rev. ST Accel. Beams 11 (2008) 104801.
- [7] A. Smolyakov et al, "Radiation Damage Studies for the Slow Extraction from SIS-100", EPAC2008, Genoa, Italy, June 2008, p. 3602 (2008).
- [8] T. Trenkler and J.B. Jeanneret, Particle Accelerators 50 (1995) 287.
- [9] J.B. Jeanneret, Phys. Rev. ST Accel. Beams 1 (1998) 081001.
- [10] M. Seidel, DESY Report, 94-103, (1994).
- [11] K. Yamamoto, Phys. Rev. ST Accel. Beams 11 (2008) 123501.
- [12] J. Beringer et al. (Particle Data Group), Phys. Rev. D86 (2012) 010001 [http://pdg.lbl.gov].
- [13] L. Sihver et al., Phys. Rev. C47 (1993) 1225.
- [14] P. Spiller, "Towards the High Intensity Limit in the FAIR Project", HB2010, Morschach, Switzerland, Sept-Oct 2010, MOIC01, p. 34 (2010).
- [15] C. Scheidenberger et al., Nucl. Instrum. Methods Phys. Res. Sect. B 142 (1998) 441.